ISSN 2522-4182

DOI: DOI: 10.32347/2522-4182.17.2025.102-118
UDC 624.012.45

EXPERIMENTAL TESTING OF A COMPLEX-GEOMETRY FLOOR SLAB MANUFACTURED USING 3DCP TECHNOLOGY

Oleg KALMYKOV[1], Petro REZNIK[2], Inna FURMAN[3], Ivan DEMIANENKO[4]

[1,2,4] O.M. Beketov National University of Urban Economy in Kharkiv, Ukraine
17, Chornoglazivska Street, Kharkiv 61002
[3]LLC "3D TECHNOLOGIES UTU"
2 Maidan Nezalezhnosti, Kyiv 01001, Ukraine
[1] oleg.kalmikov@kname.edu.ua, https://orcid.org/0000-0001-7294-4279
[2] petro.reznik@kname.edu.ua, https://orcid.org/0000-0003-3937-6833
[3] i.furman5@gmail.com, https://orcid.org/0009-0004-3012-0772
[4] ivan.demyanenko.1995@gmail.com, https://orcid.org/0000-0001-9511-7663

Abstract. This paper presents the results of an experimental investigation of a thin-walled reinforced concrete slab of complex geometry manufactured using 3D concrete printing (3DCP) technology. The aim of the study was to evaluate the stress–strain behaviour and flexural stiffness of an optimized slab whose internal structure was formed according to the principles of rational cross-sections and topology-based shape design. The tested slab, measuring 2200×2200 mm, incorporated a system of curved ribs printed in 20-mm layers, forming a cellular load-bearing pattern with enhanced material efficiency.

The experimental program was carried out on a rigid spatial steel testing frame with full perimeter support. The load was applied incrementally by placing cast-iron calibration blocks (21 kg) and heavy concrete FBS blocks weighing 518 kg, which ensured an equivalent uniformly distributed load. A total of 12 loading stages were performed with a 15-minute stabilization period at each step, reaching a maximum surface pressure of 25.06 kN/m². Vertical displacements were recorded using three high-precision dial gauges (0.01 mm accuracy), while local strains were measured by ten strain gauges with a 20 mm base installed at characteristic locations on the upper and lower surfaces of the slab.

The obtained results showed that the slab exhibited linear-elastic behaviour throughout the entire loading range. The maximum central deflection reached 2.06 mm, and after complete unloading decreased to 0.63 mm, confirming a significant proportion of recoverable deformation and the absence of damage. Strain gauge readings indicated a uniform development of compressive and tensile strains consistent with the bending moment distribution, with no evidence of localized stress concentrations.

Oleg KALMYKOV
Associate Professor, Department of Building Structures,
Assoc. Prof., PhD (Tech. Sci.)

Petro REZNIK
Associate Professor, Department of Building Structures,
Assoc. Prof., PhD (Tech. Sci.)

Inna FURMAN
LLC "3D TECHNOLOGIES UTU"
Founder

Ivan DEMYANENKO
Post-graduate student, Department of building structures

The strain curves contained no sudden jumps or anomalies, indicating the integrity of interlayer bonding and the absence of any signs of structural degradation.
The findings confirm the effectiveness of 3DCP technology for manufacturing load-bearing floor slabs with complex internal geometry. The tested element demonstrated high stiffness, reliable structural performance and highlighted the promising prospects for the development of topologically optimized reinforced concrete structures in modern construction.

Keywords: 3DCP; topology optimization; experimental testing; deflections; strains; uniformly distributed load; load-bearing capacity.

INTRODUCTION

The modern development of additive manufacturing technologies in construction is primarily associated with extrusion-based 3D printing of cementitious and concrete mixtures, which enables the creation of complex spatial geometries and significantly expands the potential for rational structural form-finding. Unlike traditional technologies, 3DCP makes it possible to eliminate formwork, reduce labor intensity, and realize topologically optimized cross-sections that ensure an efficient distribution of material according to the internal force field. Despite the rapid advancement of digital design methods and substantial progress in materials-science research related to 3D printing, experimental data on the actual structural behavior of full-scale slabs with complex geometry remain limited. This highlights the need for comprehensive testing of 3D-printed slab systems to assess their deformability, stiffness, and load-bearing capacity under real loading conditions.

ANALYSIS OF PREVIOUS RESEARCH

Review studies indicate that concrete 3D printing enables the abandonment of traditional formwork, the fabrication of complex geometries, and the adaptive control of mixture composition and toolpath trajectories. At the same time, it imposes specific requirements on rheological properties, layer formation technologies, and quality control of printed elements [1–4]. Some surveys focus on the selection of sustainable materials, optimisation of toolpath parameters, and criteria for improving the 3D printing process - all of which directly relate to rational structural shaping and the enhancement of material efficiency [3–5].

A significant share of contemporary research is dedicated to integrating digital design, topology optimisation, and digital fabrication of ribbed and funicular slabs using 3D-printed formwork. Studies conducted at ETH Zurich, TU Delft, and other research centres have demonstrated the feasibility of using 3D-printed polymer and composite formwork to create lightweight reinforced concrete slabs with complex geometry [6–13]. It has been shown that combining parametric modelling, shape optimisation, and digital fabrication technologies enables a substantial reduction in material consumption while maintaining or increasing load-bearing capacity, and allows for the creation of integrated slab systems where the geometry of ribs, voids, and zones of material concentration is aligned with the distribution of internal forces [6–13]. Parallel experimental research on shells and beams fabricated using 3D-printed polymeric or composite cementitious materials confirms the fundamental feasibility of structurally efficient shapes and their agreement with numerical models [14,15].

The theoretical foundation of rational structural shaping is grounded in the apparatus of topology optimisation developed for continuum structures [16–18]. Classical approaches - such as density-based methods, evolutionary topology optimisation, and bi-directional evolutionary optimisation (BESO) - allow for determining the material layout that minimises energy functionals or deformation criteria subject to specified constraints [16–18, 32]. Review and applied studies demonstrate the active implementation of these methods for the analysis of steel and reinforced concrete structures, including slabs, shells, and spatial systems, and highlight the connection between topology optimisation, architectural form-finding, and parametric modelling [19–21]. Against this background, Ukrainian researchers have advanced the energy-based approach to

parametric design, introducing the concept of an “energy portrait” of a structural system and using the density of strain energy as a criterion for evaluating and optimising the parameters of shells and slabs [22–25].

One of the key features of 3D-printed concrete is its layered architecture and, consequently, pronounced anisotropy of strength, stiffness, and crack resistance. Experimental studies on interlayer adhesion show a significant dependence of interface strength on the rheological properties of the fresh mix, time intervals between layers, surface condition, and extrusion parameters [26–28]. The mechanical characteristics of 3D-printed concrete are known to vary substantially in the direction of printing, along the layers, and in the vertical direction, with statistical strength parameters exhibiting clear directional dependence [26–28]. Several studies have proposed experimental procedures and statistical analysis methods to quantify anisotropy and account for it in the design of 3D-printed concrete structures [29,30], including the selection of effective design parameters and calibration of material models with regard to printing direction.

Ukrainian research makes a significant contribution to the development of resource-efficient shaping concepts for slabs and shells based on energy criteria. In particular, methods have been proposed for determining the optimal topology of reinforced concrete floor slabs with regard to the distribution of internal forces and deformations, enabling the design of rational ribbed slabs and voided systems [24,25].

Experimental evaluation of the deformability of repaired floor panels in large-panel residential buildings has confirmed the effectiveness of reconstruction strategies and provides grounds for further optimisation of structural schemes [31]. The concept of an energy portrait of a structural system has been introduced as a tool for variant-based design and shown to be applicable to reinforced concrete shells and spatial systems [25]. Additional studies demonstrate the potential of 3D printing for the fabrication of domes and monolithic beams with reinforcement, confirming the overall consistency between numerical modelling and experimental results and highlighting the prospects of integrating additive manufacturing with traditional reinforcement techniques [14,15, 33].

At the same time, the collected research indicates that most studies focus either on topology optimisation and energy-based criteria primarily for traditional reinforced concrete systems [16–22,31], or on technological and material aspects of 3D printing without direct transition to full-scale structural floor elements [1–6]. Studies concerning 3D-printed formwork and thin-walled ribbed slabs are mainly conceptual demonstrations of workflows and prototypes [6–12], whereas comprehensive integration of topology optimisation, energy analysis, and experimental verification of a 3D-printed slab with complex geometry remains insufficiently explored. Under these circumstances, the development of a methodology for designing optimised slab systems based on 3D printing - combining state-of-the-art numerical form-finding methods, energy criteria for assessing stress–strain behaviour, and experimental validation that accounts for material anisotropy - becomes highly relevant. The present study is dedicated to addressing this task.

OBJECT AND SUBJECT OF THE STUDY

The object of the study is an experimental specimen of a reinforced concrete slab of complex geometry, fabricated by concrete 3D printing (3DCP). The slab has plan dimensions of 2200×2200 mm and is formed as a spatial ribbed–cellular structure. Along the entire perimeter, a 150-mm-wide external frame is provided, ensuring contour stiffness and the transfer of support reactions.

The internal area of the slab is divided into four equal quadrants measuring 875×875 mm, within which a layer-by-layer printed curvilinear topology is formed. The total thickness of the slab is 240 mm, while the height of the internal cavities and the thickness of the printed walls vary according to the geometry of the topologically optimized profile. In the central zone, a cruciform stiffening node is arranged, ensuring the joint

structural action of the four quadrants. Reinforcement of the slab was implemented by placing steel bars between the printed layers.

The general structural layout is shown in Fig. 1. The subject of the study is the deformation behaviour of the investigated element.

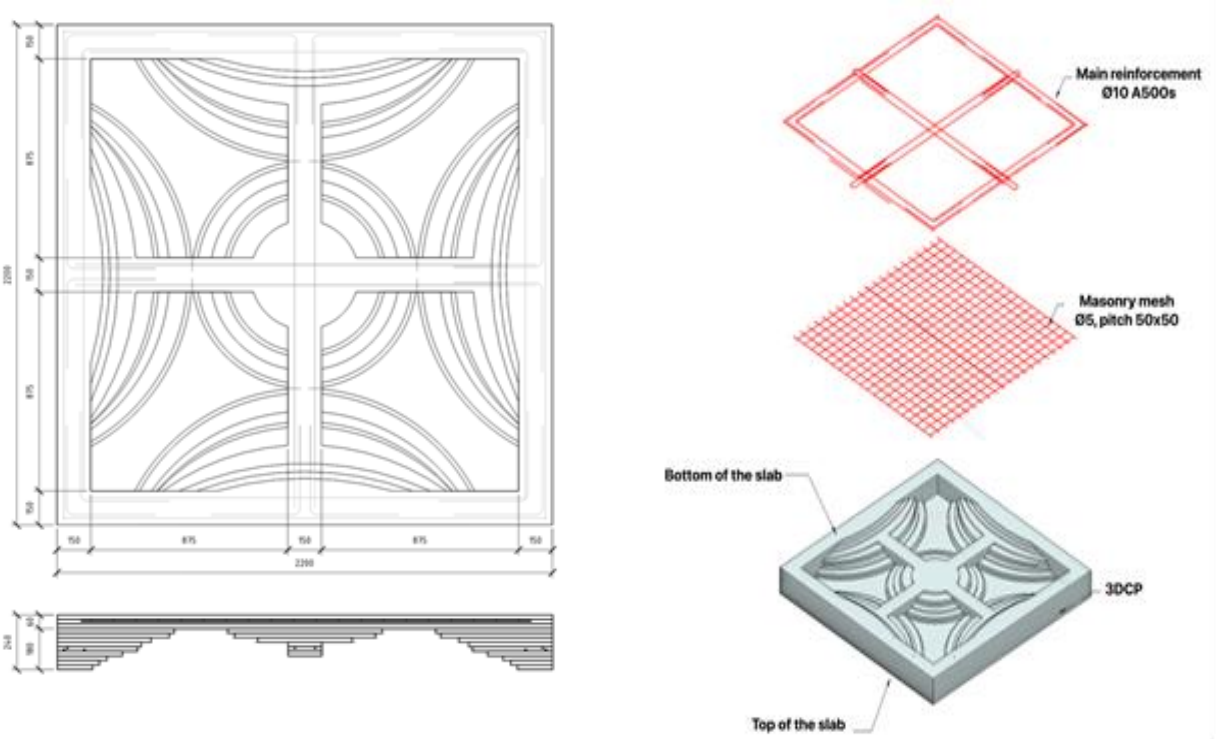

Fig. 1 Plan view, section, and axonometric representation of the experimental slab
Рис. 1 Вигляд експериментальної плити в плані, розрізі та аксонометрії

The mechan ical properties of the material used to manufacture the experimental slab were determined in a separate series of laboratory tests on specimens printed using the same layer-by-layer extrusion method as the test element. The preparation procedure, testing protocol and statistical processing of results are described in detail in [28].

Cube specimens were tested in compression in three orthogonal directions: along the extrusion path (X), perpendicular to the extrusion path (Y), and perpendicular to the printed layers (Z). The tests confirmed pronounced orthotropy of the material: the average compressive strength was 12.26 MPa in direction X, 12.44 MPa in direction Y, and 17.32 MPa in direction Z. The highest values were obtained for loading perpendicular to the layers, indicating better performance in the absence of interlayer weaknesses.

The calculated anisotropy indices were: Z/X = 1.41; Z/Y = 1.39; Y/X = 1.01, which is consistent with commonly reported characteristics of extrusion-based cementitious composites, where typical strength ratios between directions reach 1.25–1.6. The lowest coefficient of variation (CV ≈ 16%) was recorded in direction Z, confirming the stability of material properties under loading perpendicular to the printed layers.

The obtained mechanical characteristics are directly used in the analysis of the printed slab, since the material, printing technology and specimen geometry correspond to the conditions presented in [28].

LOADING SYSTEM

The load was applied to the slab in stages, with a gradual increase in intensity and regulated holding periods between steps. At the first stage, calibrated cast-iron blocks weighing 21 kg each were placed on the slab surface. The blocks were arranged in a checkerboard pattern, providing partial (approximately half) coverage of the surface. A total of 65 blocks were placed, with a combined mass of 1365 kg, corresponding to approximately 282 kg/m² (≈2.8 kN/m²).

At the second stage, additional loading was applied using the same 21 kg cast-iron blocks, which were arranged in the opposite checkerboard pattern - in the gaps between the blocks of the first stage. After this step, the entire slab surface was fully covered with 21 kg blocks. The total number of blocks reached 130 units, with a combined mass of 2730 kg, corresponding to ≈564 kg/m² (≈5.5 kN/m²).

Further load increase was achieved by placing FBS concrete blocks measuring 400×600×900 mm and weighing 518 kg each. The blocks were positioned symmetrically relative to the slab's axes, two blocks at each subsequent loading step. After each loading stage, a 15-minute holding period was implemented to allow deformation stabilization. In total, 12 loading stages were carried out (Table 1).

After reaching the seventh loading stage, the slab was held under constant load for 2 hours, followed by step-by-step unloading in the reverse order. The general view of several loading stages is shown in Fig. 2.

The slab was supported along its perimeter on a rigid testing frame designed as a spatial steel structure. The frame, assembled from rolled steel profiles, ensured stable geometry of the support contour throughout the entire loading cycle. Support was provided by the slab's edge ribs along the perimeter, reproducing the structural behavior of a slab under closed-contour support conditions.

The width of the support strip was 100 mm, which ensured a sufficient contact area between the printed ribs and the elements of the steel frame. This type of support allowed the transfer of forces from the slab to the support system without local stress concentrations and corresponded to the analytical support conditions adopted in the subsequent analysis.

Table 1 Loading stages
Табл. 1 Ступені навантаження

№	21-kg blocks, pcs.	FBS 518-kg blocks, pcs	Total mass, kg	Uniformly distributed load, kN/m²
1	65	0	1365	2.82
2	130	0	2730	5.64
3	130	2	3670	7.58
4	130	4	4610	9.52
5	130	6	5550	11.47
6	130	8	6490	13.41
7	130	10	7430	15.35
8	130	12	8370	17.29
9	130	14	9310	19.24
10	130	16	10250	21.18
11	130	18	11190	23.12
12	130	20	12130	25.06

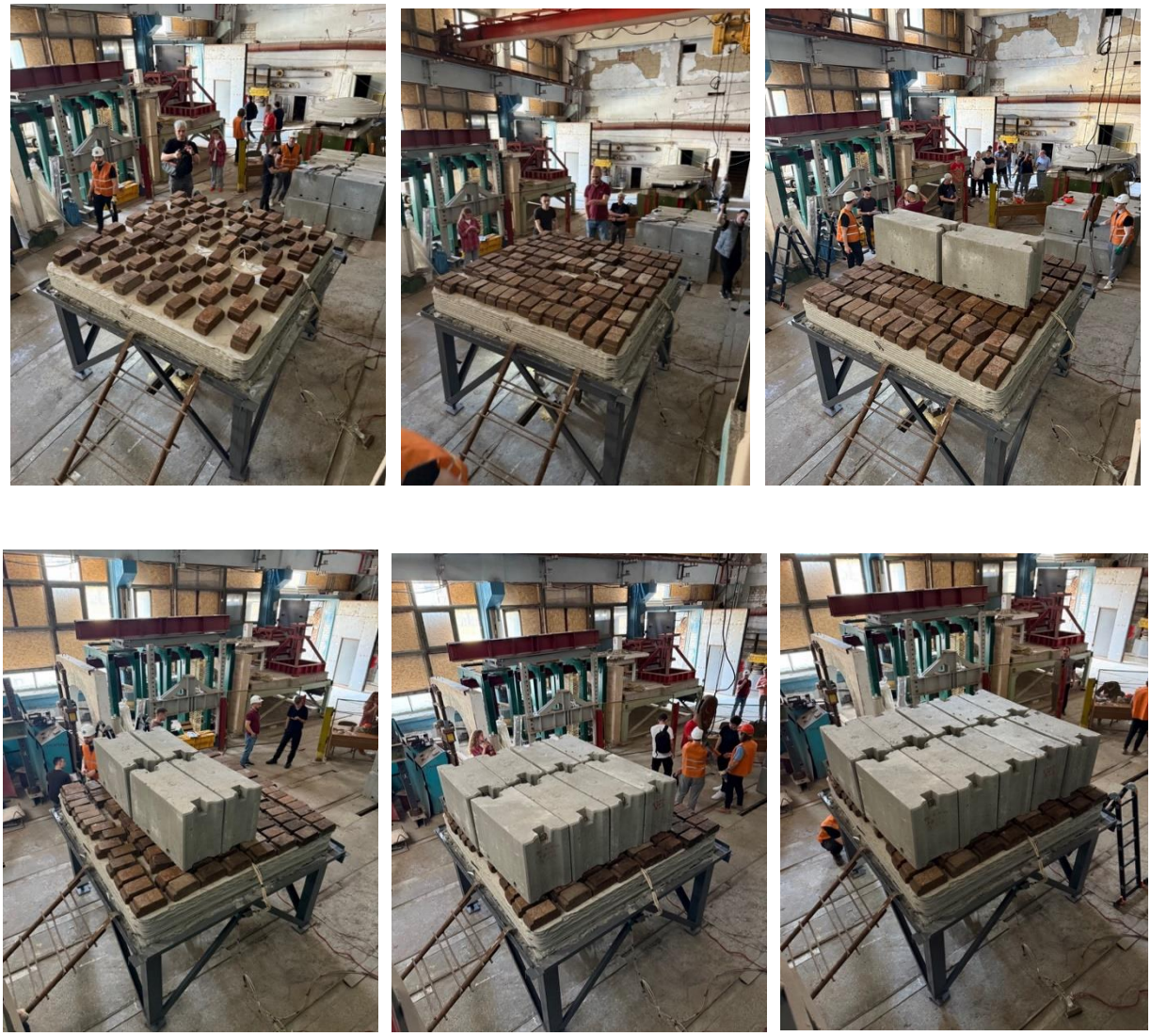

Fig. 2 Loading stages. Photo by Oleg Kalmykov
Рис. 2 Етапи завантаження. Автор фото Олег Калмиков

MEASUREMENT SYSTEM

To monitor the deformation state of the test slab during static loading, a combined measurement system was used, consisting of strain gauges and mechanical deflection gauges. Relative deformations were recorded using foil strain gauges with a 20 mm gauge length, bonded to the surface at ten characteristic locations selected according to the expected zones of maximum bending strains. The sensors were positioned on both the upper and lower surfaces of the slab; their layout was determined based on a pre-developed scheme that covered the central region, the areas near the rigid cross-shaped node, and the peripheral zones within individual quadrants, including points D-0, D-2, D-4, D-6, D-8 on the top surface, and D-10, D-12, D-14, D-16, D-18 on the bottom surface (Fig. 3a, b). This arrangement made it possible to evaluate the behaviour of the slab in both tension and compression fibres and to control section curvature during loading.

Signal acquisition from the strain gauges was performed using the multi-channel measuring system VNP-8, intended for static and repeated-static testing of structural elements.

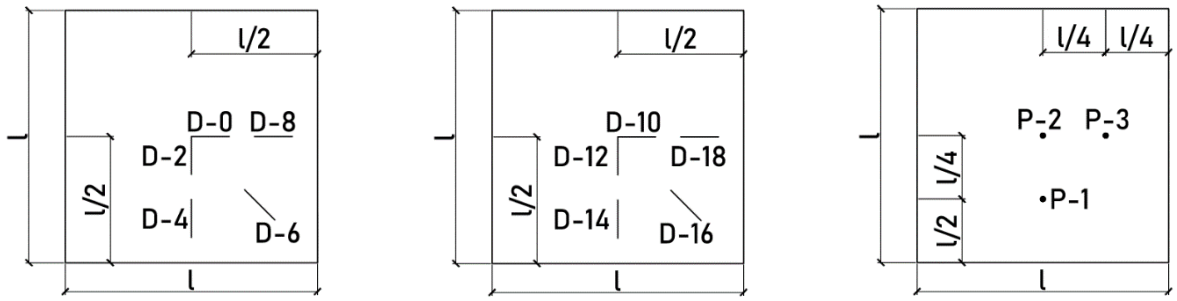

a *b* *c*

Fig. 3. Layout of measuring devices: a, b – upper and lower strain gauges, respectively; c – dial gauges
Рис. 3 Схема розташування приладів: а, б – верхні та нижні тензодатчики відповідно; в – прогиноміри

The system recorded changes in the electrical resistance of the strain gauges as digital codes within the range corresponding to resistance variations of ±9999…±39996 μΩ/Ω, depending on the configuration of the measurement bridge. For accurate conversion of electrical signals into mechanical strain, a preliminary calibration of the complete measurement chain – "strain gauge – cable – bridge – ADC"– was carried out in accordance with the procedure provided in the relevant technical documentation.

Calibration was performed on a steel cantilever beam of rectangular cross-section, onto which weights ranging from 1 to 10 kg were sequentially applied. For each load level, several measurements were taken to determine mean code values and their increments. Theoretical strains at the gauge location were calculated using the classical bending formula for prismatic members. Subsequently, the least-squares method was used to determine the conversion coefficient that linearly related the change in digital code to the magnitude of strain. This coefficient was then applied to calculate the actual strains in the test slab during loading.

In addition to strain measurements, three mechanical deflection gauges with an accuracy of 0.01 mm were used to determine the vertical displacements of the slab. They were installed at characteristic control points: P-2 - at the centre of the slab, P-3 - at the right-hand zone of the specimen, and P-1 - in the lower region, which made it possible to monitor the development of deflection in the central area and assess the symmetry of the structural response (Fig. 3c). The gauges were mounted on an independent rigid support system mechanically isolated from both the test frame and the slab, in order to eliminate the influence of frame deformations on the measurement results. The general view of the measuring devices is shown in Fig. 4.

a *b*

Fig. 4 General view of the instruments: a – dial gauges; b – strain gauges. Photo by Oleg Kalmykov
Рис. 4 Загальний вигляд приладів: а – прогиноміри; б – тензодатчики. Автор фото Олег Калмиков

RESULTS

Deflection measurement results

Deflection measurements were carried out after deformation stabilization at each loading stage, with a 15-minute holding period, which minimized the influence of initial creep of the material.

The maximum vertical displacements were recorded at the central point R2, which corresponds to the expected behavior of the slab as a bending element with maximum curvature at midspan. At the maximum uniformly distributed load of 25.06 kN/m², the deflection at point R2 reached 2.06 mm, while at points R1 and R3 the deflections were 1.65 mm and 1.93 mm, respectively (Table 2). The higher values at points R1 and R3 are attributed to local geometric features, variations in stiffness across the slab, and non-uniform rib distribution beneath the surface.

After complete unloading of the specimen, the deflection at the central point decreased by 1.43 mm, which corresponds to a residual deformation of 0.63 mm, or approximately 30% of the maximum value. A similar trend was observed at points P-1 and P-3, where the residual deflections were 0.37 mm and 0.75 mm, respectively.

Analysis of the loading–unloading curves (Fig. 5) indicates that the structure exhibits elastic–plastic behavior with a high share of recoverable deformation. The degree of shape recovery after unloading was approximately: 77% for P-1, 69% for P-2, and 61% for P-3, indicating the absence of significant plastic damage or macrocrack opening in the zones of maximum stress.

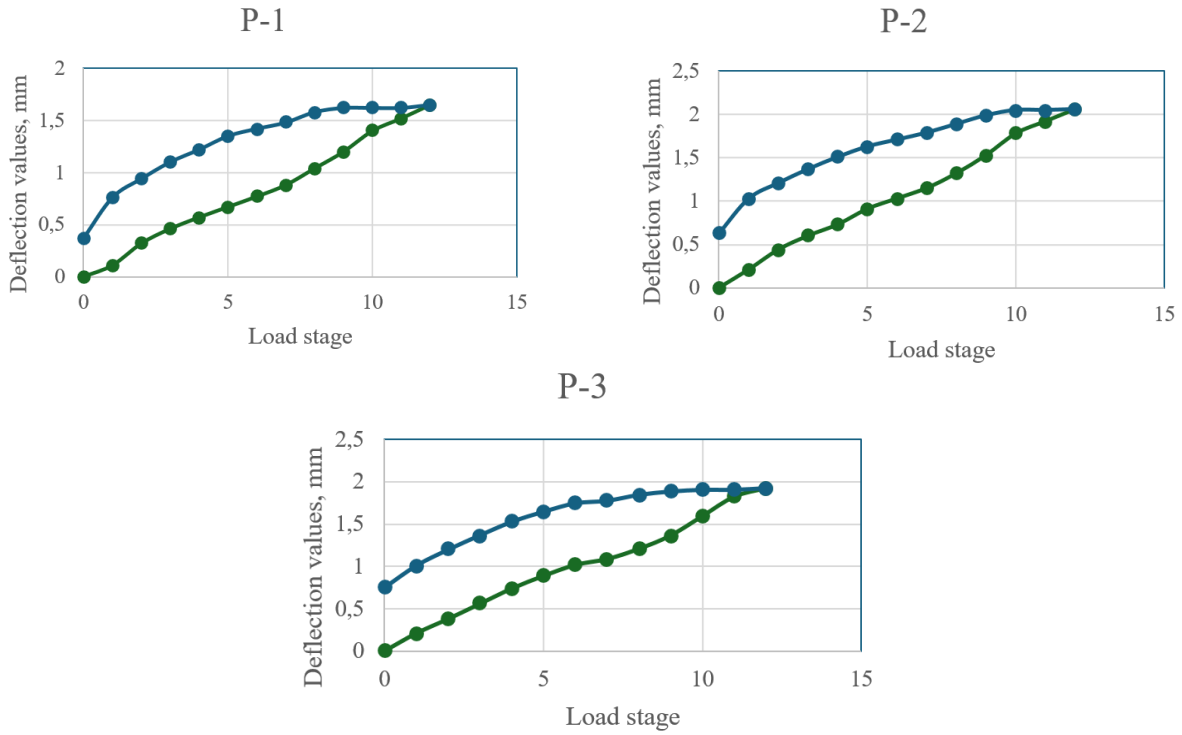

Fig. 5 Deflection values
Рис. 5 Значення прогинів

The deflection–load relationships demonstrate behavior typical for thin-walled slabs: an initial quasi-linear segment (0–10 kN/m²), followed by a gradual reduction in stiffness at loads of 10–20 kN/m², and a transition to a nearly horizontal plateau at 20–25 kN/m². The absence of sharp jumps or curve breaks confirms the integrity of the printed slab structure and the absence of brittle failure. The results are summarized in Table 2, and the graphical "load–deflection" plots are presented in Fig. 5.

The deflection–load curves exhibit a characteristic response of thin concrete slabs: the initial segment preserves an almost perfectly linear proportionality between load

and vertical displacements due to the low stress level within the structure. With further increase in load—reaching only about 25% of the structural strength limit—the curve remained close to linear with no visible stiffness degradation.

The absence of sudden drops or discontinuities confirms the integrity of the 3D-printed slab and the absence of brittle cracking at all stages.

It is important to note that the present experiment did not aim to bring the structure to complete failure, as one of its main objectives was to provide a fundamental verification of the feasibility and structural performance of floor slabs fabricated by 3D concrete printing. The results are presented in Table 2, and the load–deflection plots are shown in Fig. 5. The green curve represents loading, while the blue curve represents unloading.

Table 2 Readings of the deflection gauges
Табл. 2 Значення прогиномірів

Load stage	Load		Instrument readings, mm		
	Total, kg	Distributed, kN/m²	P-1	P-2	P-3
0	0	0	0	0	0
1	1365	2.82	0.11	0.21	0.21
2	2730	5.64	0.32	0.44	0.38
3	3670	7.58	0.46	0.6	0.56
4	4610	9.52	0.57	0.73	0.74
5	5550	11.47	0.67	0.91	0.89
6	6490	13.41	0.77	1.03	1.02
7	7430	15.35	0.88	1.15	1.09
8	8370	17.29	1.04	1.32	1.21
9	9310	19.24	1.2	1.53	1.37
10	10250	21.18	1.4	1.78	1.6
11	11190	23.12	1.52	1.92	1.83
12	**12130**	**25.06**	**1.65**	**2.06**	**1.93**
11	11190	23.12	1.62	2.05	1.91
10	10250	21.18	1.62	2.05	1.91
9	9310	19.24	1.62	1.99	1.89
8	8370	17.29	1.58	1.89	1.85
7	7430	15.35	1.48	1.79	1.78
6	6490	13.41	1.42	1.71	1.75
5	5550	11.47	1.35	1.63	1.65
4	4610	9.52	1.22	1.51	1.53
3	3670	7.58	1.1	1.37	1.37
2	2730	5.64	0.94	1.21	1.2
1	1365	2.82	0.76	1.03	1.01
0	0	0	0.37	0.63	0.75

Results of strain measurements

The deformation readings were recorded after stabilization at each loading stage, with a 15-minute holding time, which made it possible to correctly isolate the elastic component and minimize the influence of short-term creep of the printed concrete. The generalized values are presented in Table 3, and the graphical deformation curves are shown in Fig. 6.

In the areas where compressive behavior of the fibers was expected (sensors D-0, D-2, D-4, D-6), the deformations had a negative sign

(compression) and increased in magnitude with increasing load. Sensor D-0, located closer to the center, exhibited a smooth and well-linearized increase in compressive strains up to approximately -30×10^{-6} at the maximum load level.

Sensor D-2 showed slightly lower compressive amplitudes but the same stable trend, reaching values of about -35×10^{-6}.Sensors D-4 and D-6, positioned closer to the ribs of the internal topological structure, recorded the highest compressive strains (up to -70×10^{-6}), which was expected because local stiffness concentrators redistribute stresses and increase curvature in these regions.

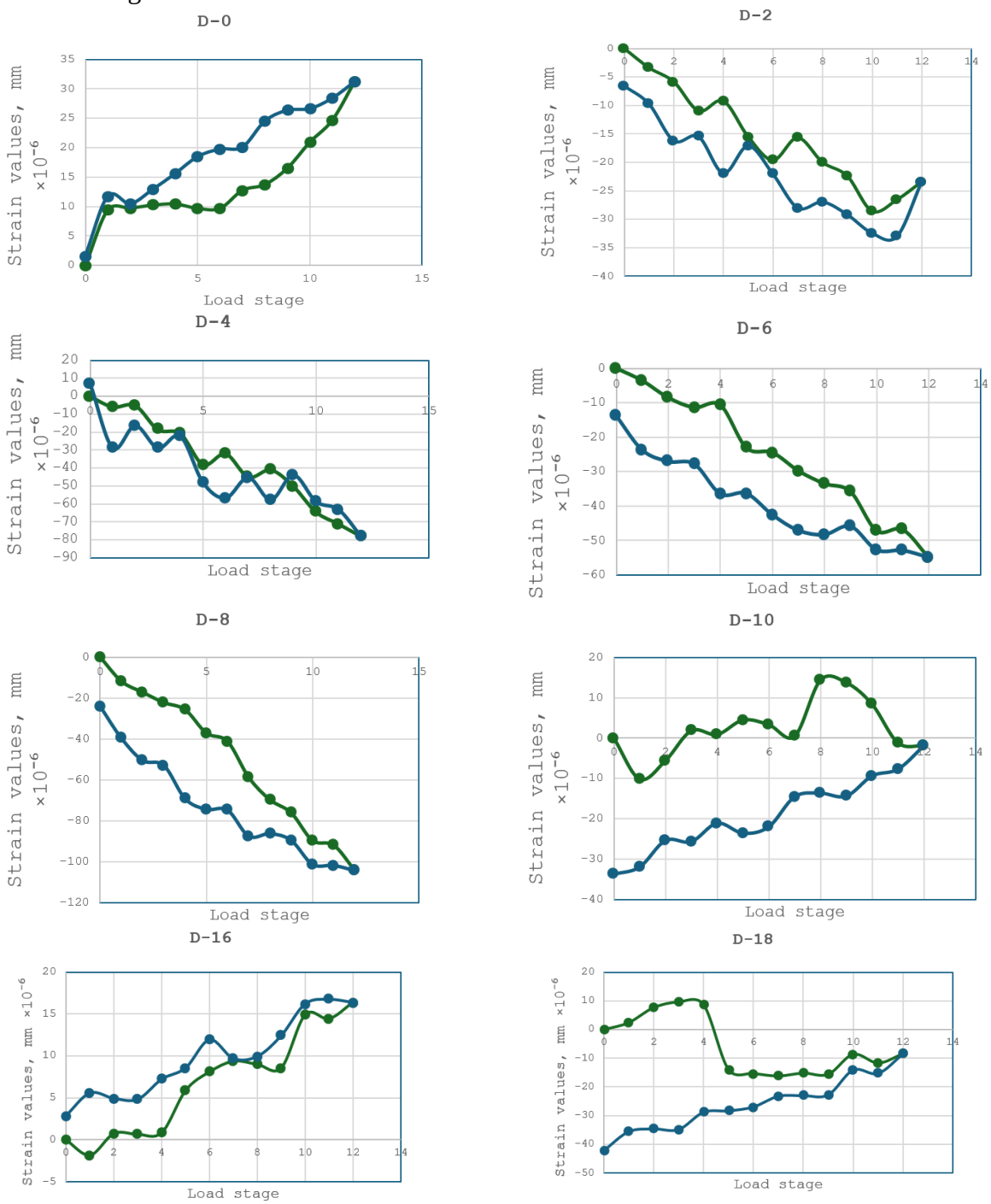

Fig. 6 Strain values
Рис. 6 Значення деформацій

Table 3. Readings of strain gauges – strains
Таблиця 3. Показання тензодатчиків – деформації

Loading stage	Strain gauges - strain values, mm ×10⁻⁶							
	D-0	D-2	D-4	D-6	D-8	D-10	D-16	D-18
0	0.00	0.00	0.00	0.00	0.00	0.00	0.00	0.00
1	9.44	-3.38	-5.86	-3.58	-11.86	-10.12	-1.80	2.44
2	9.75	-5.86	-5.09	-8.53	-17.21	-5.55	0.78	7.70
3	10.25	-10.98	-18.51	-11.38	-22.27	1.84	0.67	9.64
4	10.45	-9.23	-20.78	-10.66	-25.74	0.89	0.88	8.66
5	9.70	-15.52	-38.08	-23.10	-37.19	4.47	5.90	-13.93
6	9.70	-19.64	-32.06	-24.46	-41.30	3.32	8.11	-15.30
7	12.77	-15.68	-45.01	-29.79	-58.93	0.47	9.39	-16.19
8	13.74	-20.00	-41.08	-33.50	-69.86	14.34	9.00	-15.19
9	16.51	-22.43	-50.27	-35.79	-76.27	13.71	8.58	-15.61
10	20.92	-28.60	-64.61	-47.18	-89.79	8.37	14.92	-8.61
11	24.64	-26.60	-71.31	-46.82	-92.06	-1.17	14.43	-11.67
12	**31.19**	**-23.42**	**-78.28**	**-54.90**	**-104.56**	**-1.91**	**16.40**	**-8.40**
11	28.39	-33.03	-63.19	-52.89	-101.97	-7.69	16.76	-15.24
10	26.60	-32.45	-58.76	-52.73	-101.45	-9.33	16.23	-14.04
9	26.34	-29.18	-43.88	-45.88	-89.78	-14.36	12.44	-22.75
8	24.50	-26.96	-57.75	-48.31	-86.41	-13.62	9.96	-23.01
7	20.07	-28.01	-45.25	-47.09	-87.73	-14.51	9.70	-23.22
6	19.73	-22.05	-56.76	-42.56	-74.91	-21.95	11.95	-26.96
5	18.45	-17.10	-48.14	-36.33	-74.54	-23.54	8.58	-28.32
4	15.57	-21.91	-22.26	-36.49	-69.36	-21.05	7.24	-28.82
3	12.88	-15.46	-28.80	-27.81	-53.07	-25.64	4.84	-34.87
2	10.45	-16.20	-16.29	-27.07	-50.65	-25.33	4.94	-34.66
1	11.73	-9.72	-28.74	-23.77	-39.78	-31.91	5.59	-35.62
0	1.59	-6.55	7.29	-13.86	-24.21	-33.70	2.89	-42.25

All curves of the upper sensors exhibit a clearly monotonic behavior without jumps, inversions, or sharp anomalies, which indicates the integrity of the interlayer bond of the 3D-printed concrete and the absence of local damage or cracking during the test.

In the lower zone of the slab (sensors D-8, D-10, D-16, D-18), the deformations are predominantly tensile, which corresponds to the general bending behavior of the element. Sensor D-8 recorded the highest tensile strains (up to $+100\times10^{-6}$), which corresponds to the region of maximum curvature under bending. Sensor D-10 showed a less uniform but still elastic pattern of strain development, reaching approximately $+20\times10^{-6}$ in tension. Sensors D-16 and D-18, located in peripheral areas, demonstrated smaller but stable tensile strains, which is consistent with the actual bending pattern.

The overall behavior of the strain curves in the lower fibers exhibits an almost linear dependence in the load range of 0–20 kN/m², with minor fluctuations that may be attributed to local features of the printed-layer structure or contact stresses near the ribs.

For all sensors, after the completion of the loading cycle and subsequent unloading, the

strains returned almost entirely to values close to zero. This indicates:

- a predominantly elastic behavior of the slab;
- the absence of plastic strains in the concrete;
- no damage to the interlayer adhesion of the printed contours;
- no accumulation of deformability typical of structures with weak zones.

In fact, the strain diagrams confirm that the applied load—approximately 25 % of the strength limit of the printed concrete—did not create conditions for the development of persistent residual strains in the monitored areas.

CONCLUSIONS

The experimental testing of a slab with complex topological geometry, manufactured using layer-by-layer 3D concrete printing, confirmed the effectiveness of the selected structural concept and the suitability of 3DCP technology for producing load-bearing floor elements. The slab demonstrated stable and predictable behaviour throughout the entire range of applied loads, which reached 25.06 kN/m² (approximately 25 % of the material's strength limit), without any signs of failure, macrocrack formation, or loss of load-bearing capacity. The maximum recorded deflections were 1.65 mm at the mid-span and up to 2.06 mm in peripheral points. After completing the full loading–unloading cycle, the slab returned to a geometry close to its initial state: the residual deflections did not exceed 0.63 mm, corresponding to a 60–70 % recovery and indicating an elastic mode of structural behaviour.

The results of strain-gauge measurements correlate with the deflection data and show a monotonic and stable development of compressive and tensile strains in the corresponding zones of the slab. The maximum compressive strains in the upper fibres reached approximately -70×10^{-6}, while the tensile strains in the lower fibres were around $+100\times10^{-6}$, which corresponds to the expected behaviour of a bending structural element. After unloading, all sensors recorded an almost complete return of strain values to levels close to zero, indicating the absence of plastic damage, interlayer bond failure, or local stiffness degradation. Sensors D-12 and D-14 were excluded from the analysis due to unstable signals and inconsistency with the expected deformation patterns.

The overall stress–strain behaviour of the slab—both in terms of deflection measurements and strain-gauge data - confirms the high quality of interlayer bonding in the 3DCP material, the proper functioning of the internal ribbed structure, and the uniform transmission of loads through the topologically optimized geometry. The absence of sharp stiffness changes, strain jumps, or anomalies in the readings indicates the integrity of the printed contours and the adequate strength of the material.

The obtained results allow us to conclude that the application of 3D concrete printing technology for manufacturing floor slabs with complex internal geometry is feasible and provides a sufficient level of stiffness, load-bearing capacity, and deformability within service load ranges. The study confirms the viability of the concept and establishes an experimental basis for further scientific research, optimization of geometric parameters, and the development of design recommendations for structural elements produced using 3DCP technology.

REFERENCES

1. **Buswell, R. A., De Silva, W. L., Jones, S. Z., & Dirrenberger, J.** (2018). 3D printing using concrete extrusion: A roadmap for research. *Cement and Concrete Research, 112, 37–49*. https://doi.org/10.1016/j.cemconres.2018.05.006
2. **Liu, D., Duan, Z., Li, L., Liu, J., & Li, Z.** (2023). 3D printing concrete structures: State of the art, challenges, and opportunities. *Construction and Building Materials, 405, 133364.* https://doi.org/10.1016/j.conbuildmat.2023.133364
3. **Rehman, A. U., Kim, J. H., & Jang, J. G.** (2021). 3D concrete printing: A systematic

review of rheology, mix designs, mechanical, microstructural, and durability characteristics. *Materials, 14(14), 3800.* https://doi.org/10.3390/ma14143800

4. **Fasihi, A., Ghourchian, S., Lark, R. J., et al.** (2024). From pumping to deposition: A comprehensive review of 3D concrete printing material characterization test methods. *Construction and Building Materials, 432, 134968.* https://doi.org/10.1016/j.conbuildmat.2024.134968
5. **Zhuang, Z., Xu, F., Ye, J., et al.** (2024). A comprehensive review of sustainable materials and toolpath optimization in 3D concrete printing. npj *Materials Sustainability, 2, 12.* https://doi.org/10.1038/s44296-024-00017-9
6. **Jipa, A., & Dillenburger, B.** (2022). 3D Printed Formwork for Concrete: State-of-the-Art, Opportunities, Challenges, and Applications. *3D Printing and Additive Manufacturing, 9(2), 86–107.* https://doi.org/10.1089/3dp.2021.0024.
7. **Burger, J. J., Mata-Falcón, J., & Dillenburger, B.** (2022). Design and fabrication of optimised ribbed concrete floor slabs using large-scale 3D printed formwork. *Automation in Construction, 144, 104599.* https://doi.org/10.1016/j.autcon.2022.104599 .
8. **Mata-Falcón, J., Burger, J. J., & Dillenburger, B.** (2022). Digitally fabricated ribbed concrete floor slabs. *RILEM Technical Letters, 7, 68–78.* https://doi.org/10.21809/rilemtechlett.2022.161
9. **Jipa, A., Barentin, C., Javier, C., et al.** (2019). 3D-Printed formwork for integrated funicular concrete slabs. *In Proceedings of the IASS Symposium 2019(6), 1-10.* https://doi.org/10.3929/ethz-b-000387460
10. **Aghaei Meibodi, M., Bernhard, M., Jipa, A., et al.** (2018DF). The Smart Takes from the Strong: 3D printing stay-in-place formwork for concrete slab construction. *In E. Doubrovski, M. R. Tamke, M. R. Thomsen, et al. (Eds.), Fabricate 2017: Rethinking Design and Construction (pp. 210–217). UCL Press.* https://doi.org/10.3929/ethz-b-000237103
11. **Aghaei Meibodi, M., Jipa, A., Giesecke, R., et al.** (2018). Smart Slab: Computational design and digital fabrication of a lightweight concrete slab. *In ACADIA 2018: Recalibration: on imprecision and infidelity (pp. 434–443).* https://doi.org/10.52842/conf.acadia.2018.434
12. **Ma, J., Gomaa, M., Bao, D. W., Rezaee Javan, A., & Xie, Y. M.** (2022). PrintNervi – Design and construction of a ribbed floor system in the digital era. *Journal of the International Association for Shell and Spatial Structures, 63(2), 241–251.* https://doi.org/10.20898/j.iass.2022.017
13. **Bendsøe, M. P., & Sigmund, O.** (2004). Topology Optimization: Theory, Methods and *Applications. Springer.* https://doi.org/10.1007/978-3-662-05086-6
14. **Demchyna, B., Vozniuk, L., Surmai, M., Havryliak, S., & Famulyak, Y.** (2023). Experimental study of the dome model made using a 3D printer from PLA plastic. *AIP Conference Proceedings, 2949(1), 020025.* https://doi.org/10.1063/5.0165270
15. **Demchyna, B., Vozniuk, L., Surmai, M., Burak, D., & Shcherbakov, S.** (2024). 3D printing technology for monolithic beams with the possibility of reinforcing bars. *Bulletin of Lviv National Environmental University. Series Architecture and Construction, 25, 32–37.* [in Ukraine] https://doi.org/10.31734/architecture2024.25.032
16. **Huang, X., & Xie, Y. M.** (2010). Evolutionary Topology Optimization of Continuum Structures: Methods and Applications. *John Wiley & Sons.* https://doi.org/10.1002/9780470689486
17. **Xia, L., Xia, Q., Huang, X., & Xie, Y. M.** (2018). Bi-directional evolutionary structural optimization on advanced structures and materials: A comprehensive review. Archives of *Computational Methods in Engineering, 25(1), 437–478.* https://doi.org/10.1007/s11831-016-9203-2
18. **Stoiber, N., & Kromoser, B.** (2021). Topology optimization in concrete construction: A systematic review on numerical and experimental investigations. S*tructural and Multidisciplinary Optimization, 64(3), 1725–1749.* https://doi.org/10.1007/s00158-021-03019-6
19. **Bialkowski, S.** (2018). Topology Optimisation Influence on Architectural Design Process – Enhancing Form Finding Routine by tOpos *Toolset Utilisation. In Proceedings of the eCAADe 2018 Conference (pp. 139–148).* https://doi.org/10.52842/conf.ecaade.2018.1.139
20. **Tang, T., Wang, L., Zhu, M., Zhang, H., Dong, J., Yue, W., & Xia, H.** (2024). Topology Optimization: A Review for Structural Designs Under Statics Problems. *Materials, 17(23), 5970.*

https://doi.org/10.3390/ma17235970
21. **Hager, I., Maroszek, M., Mróz, K., et al.** (2022). Interlayer bond strength testing in 3D-printed mineral materials for construction applications. *Materials, 15(12), 4112.* https://doi.org/10.3390/ma15124112
22. **Kalmykov, O., Gaponova, L., Reznik, P., & Grebenchuk, S.** (2017). Use of information technologies for energetic portrait construction of cylindrical reinforced concrete shells. MATEC *Web of Conferences, 116, 02017*. [in Ukraine] https://doi.org/10.1051/matecconf/201711602017
23. **Shmukler, V., Petrova, O., Reznik, P., Hamad, F. S., & Sosnowska, M.** (2019). Improvement of the structural parameters of the reinforced concrete support in a mesh cage. *AIP Conference Proceedings, 2077(1), 020048.* https://doi.org/10.1063/1.5091909
24. **Kalmykov, O. O., Reznik, P. A., V'iunkovskyi, V. P., Demianenko, I. M., & Buldakov, O. O.** (2025). Towards the optimization of reinforced concrete slab topology. *Municipal Economy of Cities. Series: Information Technology and Engineering, 192, 228–235*. [in Ukraine] https://doi.org/10.33042/3083-6727-2025-4-192-228-235
25. **Shmukler, V. S., Vozniuk, L. I., & Berezhna, K. V.** (2022). Energy portrait of the structural system as a criteria for option design. *Bulletin of Kharkov National Automobile and Highway University, 98, 136–143.* [in Ukraine] https://doi.org/10.30977/BUL.2219-5548.2022.98.0.136
26. **Sanjayan, J. G., Nematollahi, B., Xia, M., & Marchment, T.** (2018). Effect of surface moisture on inter-layer strength of 3D printed concrete. *Construction and Building Materials, 172, 468–475.* https://doi.org/10.1016/j.conbuildmat.2018.03.232
27. **Skibicki, S., Dvorak, R., Pazdera, L., et al.** (2024). Anisotropic mechanical properties of 3D printed mortar by standard flexural and compression test and acoustic emission. *Construction and Building Materials, 452, 138957*. https://doi.org/10.1016/j.conbuildmat.2024.138957
28. **Reznik, P. A., Petrenko, D. H., Volodymyrov, A. V., Alataiev, D. A., & Maksymenko, V. O.** (2025). Strength anisotropy of 3d-printed concrete: experimental investigation and statistical analysis. *Scientific Bulletin of Construction, 112(1), 248–255.* [in Ukraine] https://doi.org/10.33042/2311-7257.2025.112.1.30
29. **Zhang, K., Lin, W., Zhang, Q., et al.** (2024). Evaluation of anisotropy and statistical parameters of compressive strength for 3D printed concrete. *Construction and Building Materials, 440, 1374417*. https://doi.org/10.1016/j.conbuildmat.2024.137417
30. **Panda, B., Noor Mohamed, N. A., Paul, S. C., Bhagath Singh, G., Tan, M. J., & Šavija, B.** (2019). The Effect of Material Fresh Properties and Process Parameters on Buildability and Interlayer Adhesion of 3D Printed Concrete. *Materials, 12(13), 2149.* https://doi.org/10.3390/ma12132149
31. **Kalmykov, O. O., & Binkevych, K. O.** (2024). Experimental determination of floor panels deformability of a large-panel system building after renovation. *Scientific Bulletin of Construction, 110, 42–52.* [in Ukraine] https://doi.org/10.33042/2311-7257.2024.110.1.7
32. **Kripak, V., Kolyakova, V., & Gaidai, M.** (2021). Research on the effectiveness of reinforced concrete monolithic floors with hollow liners. *Building constructions. Theory and practice,(9), 15–29.*[in Ukraine] https://doi.org/10.32347/2522-4182.9.2021.15-29
33. **Demchyna, B., Voznyuk, L., Burak, D., & Shcherbakov, S.** (2024). 3D printing of beams with the possibility of installing transverse reinforcement, taking into account the peculiarities of the construction printer. *Building construction. Theory and practice, (14), 57–66.* [in Ukraine] https://doi.org/10.32347/2522-4182.9.2021.15-29

LITERATURE

1. **Buswell, R. A., De Silva, W. L., Jones, S. Z., & Dirrenberger, J.** (2018). 3D printing using concrete extrusion: A roadmap for research. *Cement and Concrete Research, 112, 37–49.* https://doi.org/10.1016/j.cemconres.2018.05.006
2. **Liu, D., Duan, Z., Li, L., Liu, J., & Li, Z.** (2023). 3D printing concrete structures: State of the art, challenges, and opportunities. *Construction and Building Materials, 405, 133364*.

https://doi.org/10.1016/j.conbuildmat.2023.133364

3. **Rehman, A. U., Kim, J. H., & Jang, J. G.** (2021). 3D concrete printing: A systematic review of rheology, mix designs, mechanical, microstructural, and durability characteristics. *Materials, 14(14), 3800.* https://doi.org/10.3390/ma14143800
4. **Fasihi, A., Ghourchian, S., Lark, R. J., et al.** (2024). From pumping to deposition: A comprehensive review of 3D concrete printing material characterization test methods. *Construction and Building Materials, 432, 134968*. https://doi.org/10.1016/j.conbuildmat.2024.134968
5. **Zhuang, Z., Xu, F., Ye, J., et al.** (2024). A comprehensive review of sustainable materials and toolpath optimization in 3D concrete printing. npj *Materials Sustainability, 2, 12.* https://doi.org/10.1038/s44296-024-00017-9
6. **Jipa, A., & Dillenburger, B.** (2022). 3D Printed Formwork for Concrete: State-of-the-Art, Opportunities, Challenges, and Applications. *3D Printing and Additive Manufacturing, 9(2), 86–107.* https://doi.org/10.1089/3dp.2021.0024.
7. **Burger, J. J., Mata-Falcón, J., & Dillenburger, B.** (2022). Design and fabrication of optimised ribbed concrete floor slabs using large-scale 3D printed formwork. *Automation in Construction, 144, 104599.* https://doi.org/10.1016/j.autcon.2022.104599 .
8. **Mata-Falcón, J., Burger, J. J., & Dillenburger, B.** (2022). Digitally fabricated ribbed concrete floor slabs. *RILEM Technical Letters, 7, 68–78.* https://doi.org/10.21809/rilemtechlett.2022.161
9. **Jipa, A., Barentin, C., Javier, C., et al.** (2019). 3D-Printed formwork for integrated funicular concrete slabs. *In Proceedings of the IASS Symposium 2019(6), 1-10.* https://doi.org/10.3929/ethz-b-000387460
10. **Aghaei Meibodi, M., Bernhard, M., Jipa, A., et al.** (2018DF). The Smart Takes from the Strong: 3D printing stay-in-place formwork for concrete slab construction. *In E. Doubrovski, M. R. Tamke, M. R. Thomsen, et al. (Eds.), Fabricate 2017: Rethinking Design and Construction (pp. 210–217). UCL Press.* https://doi.org/10.3929/ethz-b-000237103
11. **Aghaei Meibodi, M., Jipa, A., Giesecke, R., et al.** (2018). Smart Slab: Computational design and digital fabrication of a lightweight concrete slab. *In ACADIA 2018: Recalibration: on imprecision and infidelity (pp. 434–443).* https://doi.org/10.52842/conf.acadia.2018.434
12. **Ma, J., Gomaa, M., Bao, D. W., Rezaee Javan, A., & Xie, Y. M.** (2022). PrintNervi – Design and construction of a ribbed floor system in the digital era. *Journal of the International Association for Shell and Spatial Structures, 63(2), 241–251.* https://doi.org/10.20898/j.iass.2022.017
13. **Bendsøe, M. P., & Sigmund, O.** (2004). Topology Optimization: Theory, Methods and Applications. Springer. https://doi.org/10.1007/978-3-662-05086-6
14. **Demchyna, B.H., Surmai, M., Vozniuk, L.I., Havryliak P.A.** (2023). Eksperymental-ne doslidzhennia modeli kupola, vyhotovle-noi za dopomohoiu 3D-pryntera z PLA-plastyku. *AIP Conference Proceedings, 2949(1), 020025.* https://doi.org/10.1063/5.0165270
15. **Demchyna, B., Vozniuk, L., Surmai, M., Burak D., & Shcherbakov. S.** (2024). Tekhnolohiia 3D-druku dlia monolitnykh ba-lok z mozhlyvistiu vykorystannia armatur-nykh stryzhniv. *Visnyk Lvivskoho natsiona-lnoho ekolohichnoho universytetu. Seriia «Arkhitektura ta budivnytstvo», 25, 32–37.* https://doi.org/10.31734/architecture2024.25.032
16. **Huang, X., & Xie, Y. M.** (2010). Evolutionary Topology Optimization of Continuum Structures: Methods and Applications. *John Wiley & Sons.* https://doi.org/10.1002/9780470689486
17. **Xia, L., Xia, Q., Huang, X., & Xie, Y. M.** (2018). Bi-directional evolutionary structural optimization on advanced structures and materials: A comprehensive review. *Archives of Computational Methods in Engineering, 25(1), 437–478.* https://doi.org/10.1007/s11831-016-9203-2
18. **Stoiber, N., & Kromoser, B.** (2021). Topology optimization in concrete construction: A systematic review on numerical and experimental investigations. *Structural and Multidisciplinary Optimization, 64(3), 1725–1749.* https://doi.org/10.1007/s00158-021-03019-6
19. **Bialkowski, S.** (2018). Topology Optimisation Influence on Architectural Design Process – Enhancing Form Finding Routine by tOpos Toolset Utilisation. *In Proceedings of the eCAADe 2018 Conference (pp. 139–148).* https://doi.org/10.52842/conf.ecaade.2018.1.139

20. **Tang, T., Wang, L., Zhu, M., Zhang, H., Dong, J., Yue, W., & Xia, H.** (2024). Topology Optimization: A Review for Structural Designs Under Statics Problems. *Materials, 17(23), 5970.* https://doi.org/10.3390/ma17235970
21. **Hager, I., Maroszek, M., Mróz, K., et al.** (2022). Interlayer bond strength testing in 3D-printed mineral materials for construction applications. *Materials, 15(12), 4112*. https://doi.org/10.3390/ma15124112
22. **Kalmykov, O., Haponova, L., Reznik, P., & Hrybenchuk, S.** (2017). Vykorystan-nia informatsiinykh tekhnolohii dlia enerhe-tychnoho portretnoho budivnytstva tsylin-rychnykh zalizobetonnykh obolonok. MATEC *Web of Conferences, 116, 02017***.** https://doi.org/10.1051/matecconf/201711602017
23. **Shmukler, V., Petrova, O., Reznik, P., Khammud, M., Sosnovska M. (2019).** Pokrashchennia konstruktyvnykh parametriv zalizobetonnoi opory v sitchastomu kar-kasi. *AIP Conference Proceedings, 2017 (1), 020048***.** https://doi.org/10.1063/1.5091909
24. **Kalmykov, O., Peznik, P., Viunkovskyi, V., Demianenko I., & Buldakov O.** (2025). Pro poshuk optyma-lnoi topolohii zalizobetonnoi plyty perekryttia. *Komunalne hospodarstvo mist. Seriia: Informatsiini tekhnolohii ta inzhe-neriia, 192, 228–235* https://doi.org/10.33042/3083-6727-2025-4-192-228-235
25. **Shmukler, V., Vozniuk, L.,& Berezhna. K. (2022).** Enerhetychnyi portret konstruktyvnoi systemy yak kryterii variantnoho proektu-vannia. *Visnyk Kharkivskoho natsionanoho avtomobilno-dorozhnoho universytetu, 98, 136–143.* https://doi.org/10.30977/BUL.2219-5548.2022.98.0.136
26. **Dzhei H. Sandzhaian, Bekhzad Nemato-llakhi, Min Sia, Teilor Marchment.** (2018). EVplyv poverkhnevoi volohy na mizhsharovu mitsnist betonu, nadrukovanoho za dopo-mohoiu 3d-druku. *Budivnytstvo ta budivelni materialy, 172, 468–475***.** https://doi.org/10.1016/j.conbuildmat.2018.03.232
27. **Skibicki, S., Dvorak, R., Pazdera, L., et al.** (2024). Anisotropic mechanical properties of 3D printed mortar by standard flexural and compression test and acoustic emission. *Construction and Building Materials, 452, 138957.* https://doi.org/10.1016/j.conbuildmat.2024.138957
28. **Reznik, P.A., Petrenko, D.H., Volo-dymyrov, A.V., Maksymenko, V.O., & Alataiev D.A. (2025).** Anizotropiia mitsnosti 3D-drukovanoho betonu: Eksperymentalne doslidzhennia ta statystychnyi analiz. *Naukovyi visnyk budivnytstva, 112(1), 248–255***.** https://doi.org/10.33042/2311-7257.2025.112.1.30
29. **Zhang, K., Lin, W., Zhang, Q., et al.** (2024). Evaluation of anisotropy and statistical parameters of compressive strength for 3D printed concrete. Construction and Building Materials, 440, 1374417. https://doi.org/10.1016/j.conbuildmat.2024.137417
30. **Panda, B., Noor Mohamed, N. A., Paul, S. C., Bhagath Singh, G., Tan, M. J., & Šavija, B.** (2019). The Effect of Material Fresh Properties and Process Parameters on Buildability and Interlayer Adhesion of 3D Printed Concrete. Materials, 12(13), 2149. https://doi.org/10.3390/ma12132149
31. **Kalmykov, O.O., & Binkevych K.O. (2024).** Eksperymentalne vstanovlennia deformatyv-nosti paneei perekryttiv velykopanelnoho zhytlovoho budynku pislia vidnovlennia. *Naukovyi visnyk budivnytstva, (110), 42–52.* https://doi.org/10.33042/2311-7257.2024.110.1.7
32. **Kripak, V., Koliakova, V., & Haidai, M. (2021).** Doslidzhennia efektyvnosti zalizobetonnoho monolitnoho perekryttia z porozhnystymy vkladyshamy. *Budivelni konstruktsii. Teoriia i praktyka, (9), 15–29.* https://doi.org/10.32347/2522-4182.9.2021.15-29
33. **Demchyna, B., Vozniuk, L., Burak, D. & Shcherbakov, S. (2024).** 3D druk balok iz mozhlyvistiu vlashtuvannia poperechnoho armuvannia, vrakhovuiuchy osoblyvosti ro-boty budivelnoho pryntera. *Budivelni konstruktsii. Teoriia i praktyka, (14), 57–66.* https://doi.org/10.32347/2522-4182.9.2021.15-29

ЕКСПЕРИМЕНТАЛЬНЕ ВИПРОБУВАННЯ ПЛИТИ ПЕРЕКРИТТЯ СКЛАДНОЇ ГЕОМЕТРІЇ, ВИКОНАНОЇ ЗА ДОПОМОГОЮ ТЕХНОЛОГІЇ 3DCP

Олег КАЛМИКОВ
Петро Резнік
Інна ФУРМАН
Іван ДЕМ'ЯНЕНКО

Анотація. У статті наведено результати комплексного експериментального дослідження залізобетонної тонкостінної плити складної геометрії, виготовленої методом 3D-друку бетоном (3DCP). Метою роботи є оцінювання напружено-деформованого стану, жорсткісних характеристик та загальної працездатності плити з внутрішньою структурою, сформованою на основі принципів раціонального перерізу та топологічного формоутворення. Досліджуваний зразок розміром 2200×2200 мм містив систему криволінійних ребер та комірчастих порожнин, надрукованих шарами завтовшки 20 мм. Така геометрія забезпечувала перерозподіл матеріалу відповідно до очікуваних полів напружень та мала на меті покращення конструктивної ефективності при зменшенні маси.

Випробування здійснювались на жорсткому просторовому сталевому стенді з опиранням плити по контуру. Навантаження прикладалося поетапно шляхом укладання чавунних мірних блоків масою 21 кг та важких бетонних блоків ФБС масою 518 кг, що забезпечували еквівалентне рівномірно розподілене навантаження. Загалом виконано 12 етапів навантаження з витримкою 15 хв на кожному кроці, а максимальний тиск на поверхню становив 25.06 кН/м². Геометричну деформативність контролювали трьома високоточними прогиномірами (0.01 мм), тоді як локальні деформації фіксували десять тензометричних датчиків із базою 20 мм, наклеєних у характерних зонах верхньої та нижньої поверхонь плити.

Аналіз отриманих результатів показав, що плита працює у межах лінійно-пружної деформативності в усьому діапазоні навантажень. Максимальний прогин у центрі досяг 2.06 мм, а після повного розвантаження зменшився до 0.63 мм, що підтверджує значну частку зворотних деформацій та відсутність пошкоджень у матеріалі. Показання тензодатчиків засвідчили рівномірний розвиток стискаючих і розтягуючих деформацій, їх кореляцію з полем згинальних моментів та відсутність локальних зон концентрації напружень. Деформаційні криві не містили стрибків або аномалій, що вказує на цілісність міжшарових з'єднань і відсутність ознак руйнування.

Отримані результати підтверджують ефективність застосування технології 3DCP для створення несучих плит перекриття складної внутрішньої структури, демонструють високу жорсткість та надійність друкованого елемента й підкреслюють перспективи розвитку топологічно оптимізованих залізобетонних конструкцій у сучасному будівництві.

Ключові слова: 3DCP; топологічна оптимізація; експериментальне випробування; прогини; деформації; рівномірно розподілене навантаження; несуча здатніст.

Received: October 28, 2025.
Accepted: November 30, 2025